Structural displacement estimation using accelerometer and FMCW millimeter wave radar

Zhanxiong Ma [a], Jaemook Choi [a], Liu Yang [a,b], Hoon Sohn [a,*]

[a] Department of Civil and Environmental Engineering, Korea Advanced Institute of Science and Technology, Daejeon, South Korea
[b] Department of Civil and Environmental Engineering, The Hong Kong University of Science and Technology, Clear Water Bay, Kowloon, Hong Kong

ARTICLE INFO

ABSTRACT

Structural displacement plays a crucial role in structural health monitoring. However, its measurement remains challenging for many civil infrastructure applications. This study proposes a structural displacement estimation technique that fuses measurements from a collocated accelerometer and frequency-modulated continuous-wave millimeter wave radar at displacement estimation location on a structure. Automated initial calibration was first performed using short-period (less than 1 min) radar and acceleration measurements. The best target is automatically selected from the surroundings, and a conversion factor to convert the line-of-sight displacement to the structural displacement in the actual vibration direction is automatically estimated for the target. After calibration, the displacement is estimated in real time from radar measurements using the selected best target and its estimated conversion factor. Note that an accelerometer-aided phase-unwrapping algorithm is proposed and applied to address the phase-wrapping issue when the structural displacement is larger than the radar wavelength. The radar-based displacement is further fused with the acceleration measurement using a finite impulse response filter to estimate the displacement with improved accuracy at the cost of a short time delay. Laboratory tests on a four-story building model and a field test on a pedestrian bridge were conducted to validate the proposed displacement estimation technique. The displacements estimated by the proposed technique had an error of less than 1 mm in both tests compared to the ground-truth displacements measured by laser-based displacement sensors.

1. Introduction

Displacement response plays a crucial role in structural health monitoring because it helps to understand the global behavior of a structure, assess structural safety, and can be used for structural control and disaster prevention and mitigation. Displacement has been directly considered in structural design codes of several countries as a safety indicator [1–3]. For example, the bridge design code in the United States requires the bridge displacement to be less than 1/1000 of the bridge length under normal vehicle and pedestrian loads [1]. In addition, displacement response has been used for bridge loading rating [4], system identification [5], and finite element model updating [6]. Therefore, it is essential to monitor structural displacement. Note that that the displacement discussed in this study is the displacement relative to a fixed ground.

In practice, accelerometers are commonly used for structural displacement estimation. The displacement can be easily obtained

* Corresponding author.
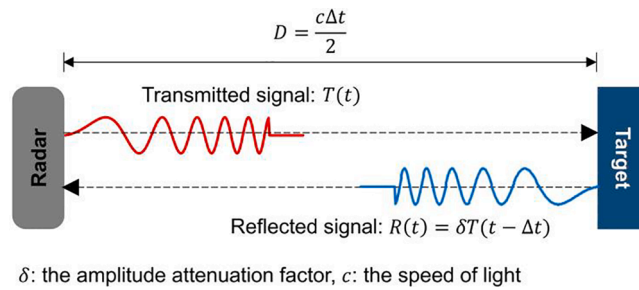 *E-mail address:* hoonsohn@kaist.ac.kr (H. Sohn).

Fig. 1. Overview of frequency-modulated continuous-wave (FMCW) radar ranging.

from acceleration measurements using double integration. However, the double integration process can amplify the measurement noise in acceleration measurements, and a large low-frequency drift is commonly observed in acceleration-based displacements. Note that the drift induced by the accelerometer measurement noise may be reduced by using a quiet accelerometer, but cannot be fully avoided. Several techniques, including finite impulse response (FIR) filters [7–9] and a state-space approach [10], have been developed to remove such drift, but these techniques also remove low-frequency structural displacement.

Displacement can also be directly measured with linear variable differential transformer (LVDT), real-time kinematic global navigation satellite system (RTK-GNSS), laser Doppler vibrometer (LDV), and vision cameras. However, the application of LVDT is limited to small-scale structures and short time measurement due to the use of a temporary scaffold, and its measurement accuracy is very sensitive to scaffold vibration. Though RTK-GNSS is applicable to large-scale structures, it has a limited accuracy of around 10 mm, and its sampling rate is only up to 20 Hz. LDV is rather expensive and not suitable for long-term continues displacement monitoring. As for vision cameras, their displacement measurement accuracy is highly affected by light and weather conditions. In addition, they are not suitable for long-term continuous monitoring due to high-computational costs.

Efforts have been made to fuse accelerometers with other types of sensors that can measure or estimate the displacement to obtain an improved displacement [11–19]. Examples include the fusion of a RTK-GNSS and accelerometer [11], and the fusion of strain sensors and accelerometers [12,13]. However, the former does not work in a GNSS-denied environment and may suffer from low accuracy due to multi-path errors; the latter only works for beam-like structures and may have large errors when the mode shapes of a target structure differ significantly from the assumed mode shapes. The fusion of vision cameras and accelerometers has also been explored [14,18,19], but the displacement estimation accuracy is significantly affected by weather and light conditions.

Radar systems have been studied for over a decade for structural displacement measurement. A radar system transmits a frequency-modulated signal and receives a signal reflected by an object. The displacement is estimated in the line-of-sight (LOS) direction from the time delay between the transmitted and received signals. Radar systems are not affected by weather or light conditions and have been used to monitor displacements of long-span bridges [20], pedestrian bridges [21,22] traffic light structures [23], etc. In these applications, centimeter wave radars with a radio frequency (RF) within 30 GHz were used. Currently, millimeter wave (mmWave) radar has been developed and is a promising technique for measuring small displacements owing to its short wavelength [24]. In addition, mmWave radar is small, lightweight, low-powered, cost-efficient, and suitable for any extreme weather [25]. However, there are the following limitations when measuring structural displacement using mmWave radar. First, a manual initial calibration is required to identify the locations of radar-detected targets and estimate the conversion factors necessary for converting the LOS displacements to structural displacements in an actual vibration direction. In addition, the raw phase directly extracted from the radar measurement is constrained to the range of $[-\pi, \pi]$, and phase wrapping occurs when the true phase is outside this range, resulting in inaccurate displacement estimation.

This study proposes a continuous structural displacement estimation technique using the fusion of frequency-modulated continuous-wave (FMCW) mmWave radar and acceleration measurements. Automated initial calibration was first performed using short-period (less than 1 min) radar and acceleration measurements to select the best target from the surroundings, and estimate its conversion factor for converting the LOS displacement to the structural displacement in an actual vibration direction. After the calibration, the displacement is estimated in real time from radar measurement using the selected best target and its estimated conversion factor, and the radar-based displacement is further fused with acceleration measurement using an FIR filter to estimate the displacement with an improved accuracy at the cost of a short time delay. The main contributions of this study include: (1) collocated FMCW mmWave radar and accelerometer at displacement estimation location on a structure are fused for structural displacement estimation, (2) the best target necessary for radar-based displacement estimation is automatically selected from the surroundings, (3) an accelerometer-aided phase-unwrapping algorithm is developed to recover the unwrapped phase from the radar measurement, and the LOS displacement is estimated from the radar measurement using the unwrapped phase, and (4) a conversion factor necessary for converting the LOS displacement to structural displacement in an actual vibration direction is automatically estimated.

The remainder of this paper is organized as follows. The FMCW radar ranging principle and conventional structural displacement estimation using an FMCW radar are briefly presented in Section 2, and Section 3 illustrates the working principle of the proposed technique. The validation of the proposed technique on a four-story building model and a pedestrian bridge is presented in Section 4 and Section 5, respectively. Concluding remarks are provided in Section 6.
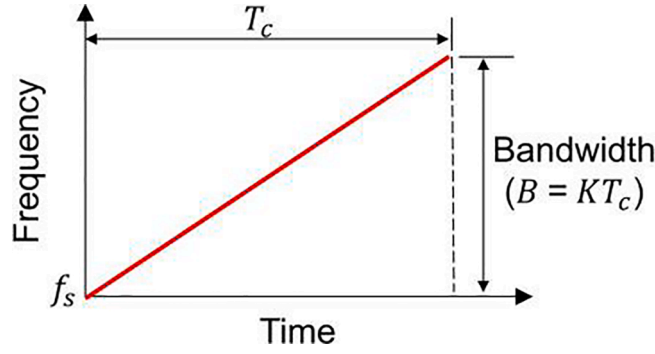
Fig. 2. Frequency-modulated signal.

2. Overview of FMCW radar-based displacement estimation

2.1. FMCW radar ranging principle

An overview of the FMCW radar ranging is shown in Fig. 1. Radar transmits a frequency-modulated signal and receives a signal reflected by a target. By extracting the time delay (Δt) between the transmitted and reflected signals, the distance (D) between the radar and the target is estimated,

$$D = \frac{c\Delta t}{2} \tag{1}$$

where c denotes the speed of light.

Several different frequency-modulated signals can be used as transmission signals, and the one employed in this study was a chirp signal [24],

$$T(t) = e^{j\left(2\pi f_s t + \pi K t^2\right)} \tag{2}$$

and thereafter the reflected signal becomes,

$$R(t) = \delta T(t - \Delta t) = \delta e^{j\left(2\pi f_s(t - \Delta t) + \pi K(t - \Delta t)^2\right)} \tag{3}$$

where f_s, K, and T_c denote the start frequency, frequency slope, and time duration of the chirp signal, respectively (Fig. 2). δ denotes the amplitude attenuation factor.

To extract the time delay (Δt), an intermediate frequency (IF) signal is defined as:

$$IF(t) = T(t) \times R^*(t) \approx \delta e^{j(\varphi + \omega t)}, \, 0 < t < T_c \tag{4}$$

$$\omega = 2\pi K \Delta t$$

$$\varphi = 2\pi f_s \Delta t$$

Thus, Δt can be extracted from either the frequency (ω) or phase (φ) of the IF signal. Note that $R^*(t)$ denotes the complex conjugate of $R(t)$. By combining Equation (1) and Equation (4), the distance can be estimated as follows:

$$D = \frac{c}{4\pi K}\omega = \frac{c}{4\pi f_s}\varphi \tag{5}$$

Note that the above explanation is based on a single target, and in the case of multiple targets, the reflected signal (Equation (3)) becomes:

$$R(t) = \sum_{m=1}^{Q} \delta^m e^{j\left\{2\pi f_s(t - \Delta t^m) + \pi K(t - \Delta t^m)^2\right\}} \tag{6}$$

and IF signal (Equation (4)) becomes,

$$IF(t) \approx \sum_{j=1}^{Q} \delta^m e^{j(\varphi^m + \omega^m t)} \tag{7}$$
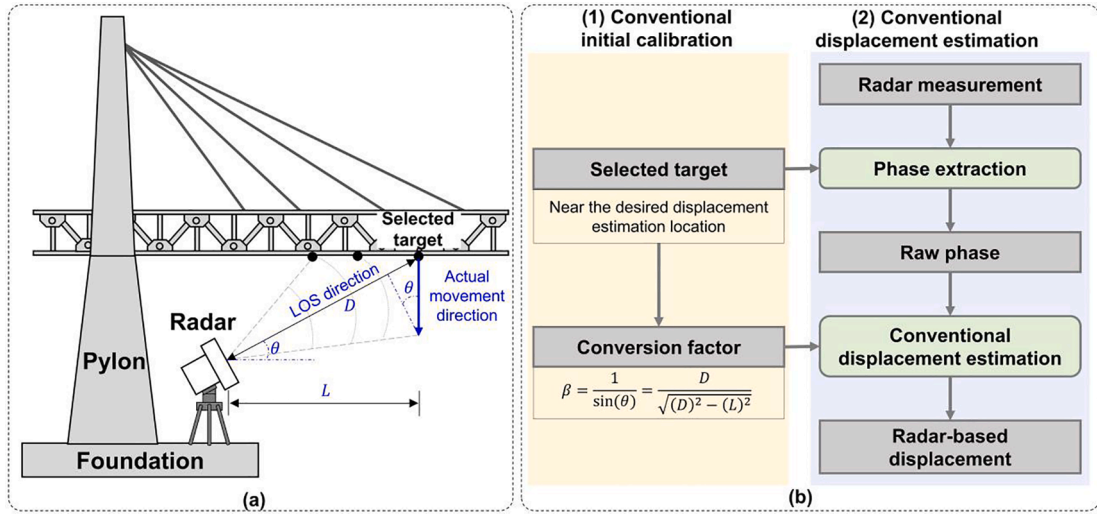
$$\omega^m = 2\pi K \Delta t^m$$

Fig. 3. Overview of conventional structural displacement estimation using a FMCW radar: (a) sensor setup and (b) overall flowchart for displacement estimation.

$$\varphi^m = 2\pi f_s \Delta t^m$$

where δ^m is the amplitude attenuation factor of the mth target. Δt^m is the time delay between the transmitted signal and reflected signal from the mth target, and Q is the number of targets. Similarly, the distance for the mth target can be estimated from either the frequency or the phase:

$$D^m = \frac{c}{4\pi K}\omega^m = \frac{c}{4\pi f_s}\varphi^m \tag{8}$$

2.2. Conventional structural displacement estimation using FMCW radar

Fig. 3 shows sensor setup and overall flowchart of the conventional structural displacement estimation technique using a FMCW radar. A radar is installed at a fixed location near a structure of which displacement is to be estimated (Fig. 3(a)). By continuously estimating distances between the radar and detected targets, distance variances from initial distances become displacements of these targets [20]. Note that the phase extracted from radar measurement is more sensitive and thereby used here for displacement estimation. The radar usually detects multiple targets (*i.e.,* the different parts of the structure), and estimates the displacement of each target in a LOS direction. Therefore, an initial calibration is first, manually performed to select a target near the location where displacement to be estimated and estimate a conversion factor for the target to convert the LOS displacement to the displacement in the actual vibration direction. Thereafter, displacement is continuously estimated in the actual vibration direction using the selected target and the estimated conversion factor. (Fig. 3(b)). Note that in the case of multiple displacement estimation, multiple targets should be selected. More details are explained below:

(1) **Conventional initial calibration:** The radar transmits a frequency-modulated signal and receives a signal reflected by multiple targets. Based on the radar ranging principle, as explained in Section 2.1, the LOS distance between these targets and the radar was estimated. The locations of these targets on the structure were identified using a laser rangefinder, and a target near the desired displacement estimation location was selected. Subsequently, a conversion factor is estimated for the target from the geometric relationship between the radar and selected target [20],

$$\beta = \frac{D}{\sqrt{(D)^2 - (L)^2}} \tag{9}$$

where D and L denote the distances between the radar and selected target in the LOS and horizontal directions, respectively.

(2) **Conventional displacement estimation:** The radar continuously transmits a chirp signal and receives a reflected signal. At each time step (*e.g.,* the kth time step), the phase corresponding to the selected target (φ_k) is extracted from the radar measurement. Once the LOS distance between the radar and target is estimated from the extracted phase, the variation in the initial distance (D_0) becomes the LOS displacement. Finally, the LOS displacement was converted to the displacement in the actual vibration direction (u_k) using the previously estimated conversion factor (β):

$$u_k = \beta(D_k - D_0) = \beta\frac{c}{4\pi f_s}(\varphi_k - \varphi_0) \tag{10}$$
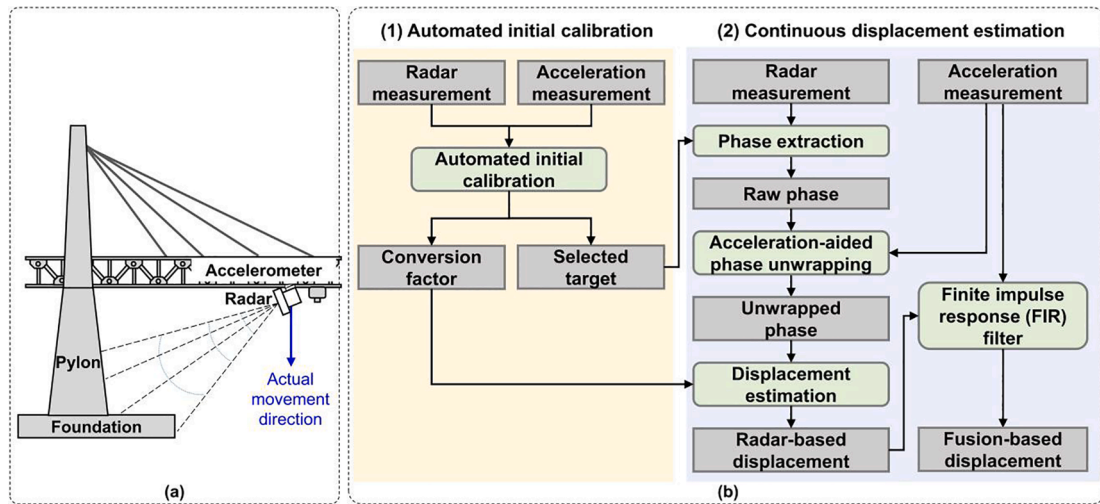
Fig. 4. Overview of the proposed displacement estimation technique using mmWave radar and accelerometer: (a) sensor setup and (b) overall flowchart for displacement estimation.

where φ_0 denotes an initial phase.

However, the conventional technique has the following limitations. First, the conventional techniques commonly installed radar sensors at a fixed location, but securing such installation location for long-term monitoring can be challenging because the radar sensor can be stolen or damaged when it is permanently installed in public open space. Cabling for permanent power supply and data retrieval can be issues, and getting permission to install the radar in privately owned properties can be difficult. Second, there is no guarantee that a stable refection could be obtained from the displacement estimation location of the target structure. In such cases, an artificial reflector needs to be placed at displacement estimation location. Third, to select a target near the desired displacement estimation location, the locations on the structure of all targets detected by the radar should be identified, which is cumbersome in practice. In addition, estimating the conversion factor is cumbersome because the horizontal distance between the selected target and the radar needs to be manually measured. Last, the raw phase directly extracted from the radar measurement is constrained to the range of $[-\pi, \pi]$, and phase wrapping occurs when the true phase is outside this range. Based on the relationship between phase and displacement given in Equation (5), the estimated displacement is constrained to $[-1/4\ \lambda, 1/4\ \lambda]$. Here, λ denotes the radar wavelength. Actual structures commonly have displacement outside of this range, and therefore their displacements cannot be correctly estimated from the raw phase.

3. Development of structural displacement estimation technique based on FMCW mmWave radar and accelerometer measurements

To address the limitations of only using radar, this study proposes a new displacement estimation technique using an FMCW mmWave radar and accelerometer. As shown in Fig. 4(a), an mmWave radar (including transmitter and receiver) and accelerometer are placed at the same location, that is, the displacement estimation location, eliminating the need for a fixed installation location for long-term continues monitoring. Because the radar is installed at the displacement estimation location, multiple targets will be available within the field of view of the radar, and the best target with stable reflection can be selected for displacement estimation. The collocated installation of the radar and accelerometer on the structure also allows for the fusion of two sensors, which offers following additional benefits: (1) automatic selection of the best target required for radar-based displacement estimation, (2) automatic estimation of the conversion factor, (3) adaptive phase unwrapping, and (4) improved displacement estimation accuracy. A flowchart of the proposed technique is shown in Fig. 4(b) and consists of two parts.

(1) **Automated initial calibration:** Radar and acceleration measurements were initially collected for a short period (less than 1 min) to automatically select the best target and estimate its conversion factor. Further details are provided in Section 3.1.

(2) **Continuous displacement estimation:** The raw phase corresponding to the best target is measured using radar, and an acceleration-aided phase-unwrapping algorithm is developed to recover the true phase from the raw phase. More details of the algorithm are provided in Section 3.2. Thereafter, the radar-based displacement was estimated in the actual vibration direction using the unwrapped phase and the estimated conversion factor (β). Finally, the radar-based displacement was fused with the acceleration measurement using an FIR filter to obtain a fusion-based displacement with improved accuracy (Section 3.3).

3.1. Automated best target selection and conversion factor estimation

In this section, automated initial calibration is performed to select the best target and estimate the conversion factor of the target.
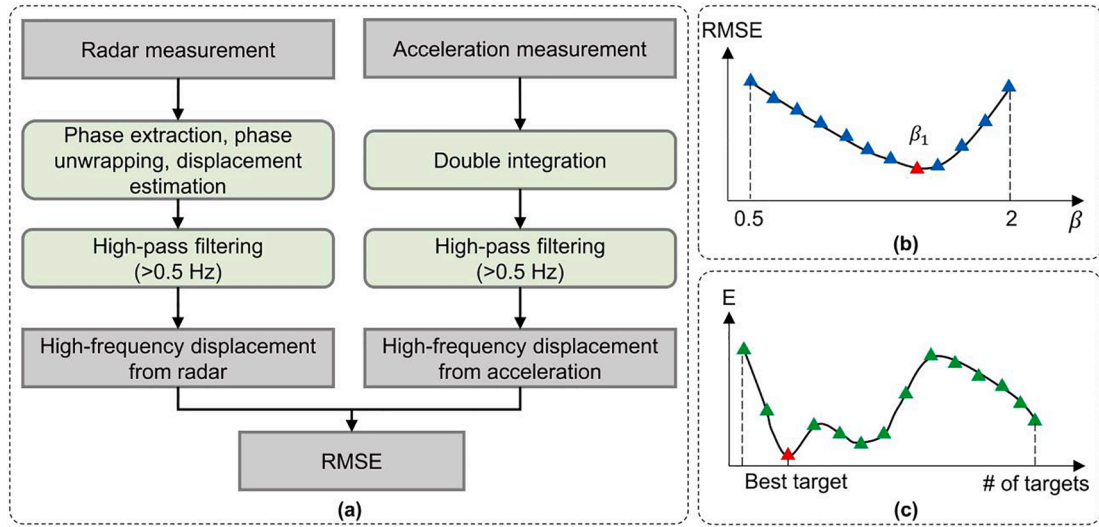
Fig. 5. Automated best target selection and conversion factor estimation: (a) Step 1: RMSE estimation for target 1 using an initial conversion factor of 0.5, (b) Step 2: selection of best conversion factor by repeating Step 1 with different conversion factor values, and (c) Step 3: best target selection by repeating Steps 1 and 2 for all targets.
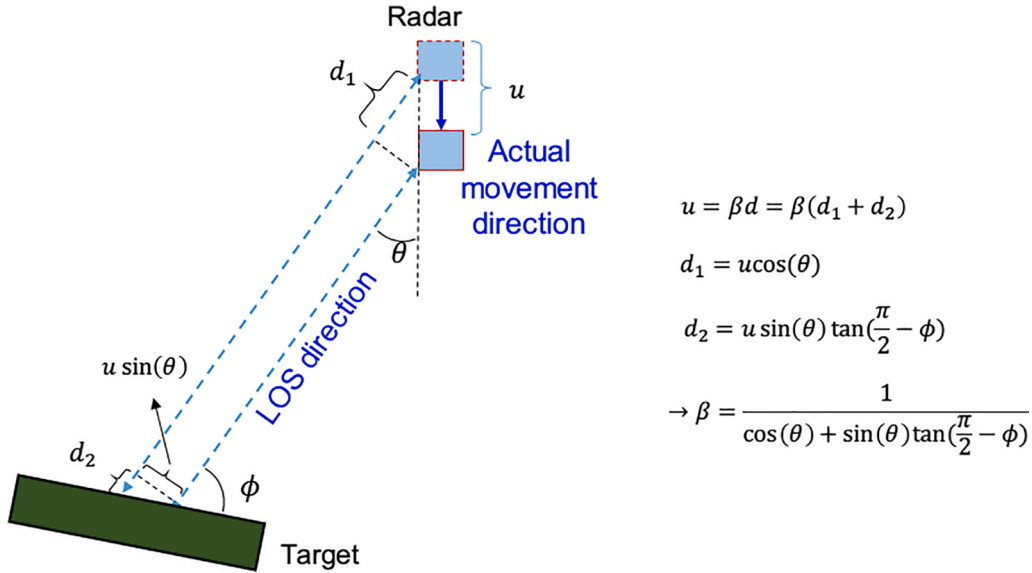

$$u = \beta d = \beta(d_1 + d_2)$$

$$d_1 = u\cos(\theta)$$

$$d_2 = u\sin(\theta)\tan\left(\frac{\pi}{2} - \phi\right)$$

$$\rightarrow \beta = \frac{1}{\cos(\theta) + \sin(\theta)\tan\left(\frac{\pi}{2} - \phi\right)}$$

Fig. 6. Definition of the conversion factor with a generalized geometric relationship between a radar and a target.

The high-frequency displacement from acceleration is used as the reference, and the selection of the best target and estimation of its conversion factor are performed by minimizing the root-mean-square error (RMSE) of the high-frequency displacement from the radar with respect to the reference. The detailed procedure is shown in Fig. 5, and consists of three steps.

Step 1: Select target 1, set an initial value (0.5 in this study) for its conversion factor, and calculate the RMSE between two high-frequency displacements independently estimated from radar and acceleration measurements (Fig. 5(a)). Note that the displacement estimated from acceleration through double integration has a large low-frequency drift, and the purpose of using high-pass filtering with a cut-off frequency of 0.5 Hz is to remove the drift. The value of 0.5 Hz is determined for the accelerometer used in this study (EpiSensor ES-U2) after a series of laboratory tests. A different value could be used if other accelerometers are used.

Step 2: Obtain the RMSE vs conversion factor curve by gradually varying the conversion factor value from 0.5 to 2 and repeating Step 1. The conversion factor corresponding to the smallest RMSE was selected as the final value (Fig. 5(b)). The smallest RMSE value is denoted as E, which is used later for the best target selection.

Step 3: Repeat Steps 1 and 2 to obtain the E values and conversion factors for all targets, and the target with the smallest E value is defined as the best target (Fig. 5(c)). The selected best target and its estimated conversion factor were used for continuous
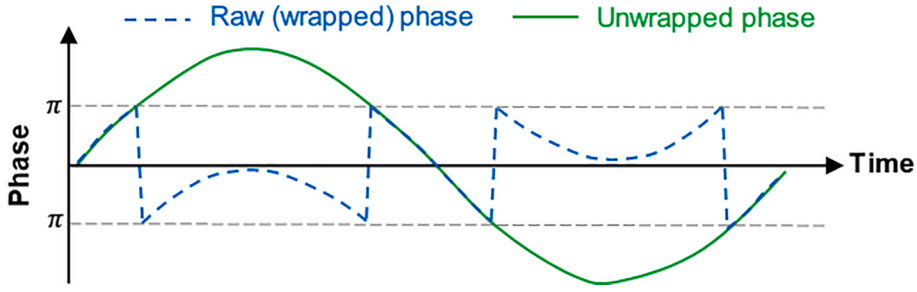
Fig. 7. Simple example of the wrapped and unwrapped phases.

displacement estimation.

There are two things that need to be mentioned. First, Fig. 6 shows the definition of the conversion factor considering a generalized geometric relationship between a radar and a target. The conversion factor (β) should be defined as,

$$\beta = \frac{1}{\cos(\theta) + \sin(\theta)\tan\left(\frac{\pi}{2} - \phi\right)} \tag{11}$$

where θ denotes the angle between the actual movement direction and the LOS direction, and ϕ denotes the angle between the LOS direction and the surface of the target. In practice, the θ value can be calculated by measuring vertical and LOS distances between the radar and the target using a laser rangefinder, but it is difficult to obtain the ϕ value. Thus, the simplified equation (Equation (9)) was used in existing techniques to define the conversion factor. Note that, the proposed technique estimates the conversion factor using initial radar and acceleration measurements without knowing the values of ϕ and θ. Second, it is apparent that the selected best target should have no self-movement. In addition to that, the best target should have a flat surface. As shown in Fig. 6, the conversion factor was assumed to be constant and the assumption was valid only when the target has a flat surface. In cases that the target has a curved or rough surface, the conversion factor is not constant and using a constant conversion factor will introduce errors in the estimated displacement. Note that, though displacement may be better estimated with an artificial-designed reflector, the installation of such a reflector may not be convenient in real applications.

3.2. Accelerometer-aided phase-unwrapping algorithm

Phase wrapping can be a serious problem when the structural displacement is larger than the radar wavelength, thus causing inaccurate displacement estimation. The existing phase-unwrapping algorithm [26] assumes that the phase change between any consecutive time steps is smaller than π. For each time step, if the phase jump relative to the previous time step is greater than or equal to π, the phase is shifted by adding multiples of $\pm 2\pi$ until the phase jump is less than π. A simple example of the wrapped and unwrapped phases is shown in the Fig. 7. However, the assumption may not always be valid, and then causes incorrect phase unwrapping.

This section proposes an accelerometer-aided phase-unwrapping algorithm to overcome this limitation. At each time step (*e.g.,* the kth time step), the displacement is first predicted using the displacement estimation at the $(k-1)^{\text{th}}$ and $(k-2)^{\text{th}}$ time steps (*i.e.,* u_{k-1} and u_{k-2}) and acceleration at the $(k-1)^{\text{th}}$ time step (a_{k-1}),

$$\widehat{u}_k = 2u_{k-1} - u_{k-2} + (\Delta t)^2 a_{k-1} \tag{12}$$

Thereafter, the phase is predicted as,

$$\widehat{\varphi}_k = 4\pi f_s \frac{\widehat{u}_k}{\beta c} \tag{13}$$

Assuming that the raw phase is extracted as φ_k, the unwrapped phase is as follows:

$$\{\varphi_k \pm 2p\pi\} \tag{14}$$

where p is an integer. Finally, the unwrapping phase ($\overline{\varphi}_k$) is estimated as the one in this list and is closest to the predicted phase ($\widehat{\varphi}_k$),

$$\overline{\varphi}_k = \varphi_k + 2\pi \times round\left(\frac{\widehat{\varphi}_k - \varphi_k}{2\pi}\right) \tag{15}$$

The radar-based displacement is then estimated using the unwrapped phase ($\overline{\varphi}_k$) instead of the raw phase φ_k,

$$u_k = \beta \frac{c}{4\pi f_s}(\overline{\varphi}_k - \varphi_0) \tag{16}$$

Note that it is assumed that the test structure does not vibrate or vibrates weakly during the initial two time step and then phase wrapping does not occur. This can be achieved by setting the start point to a time point where the acceleration is very small.
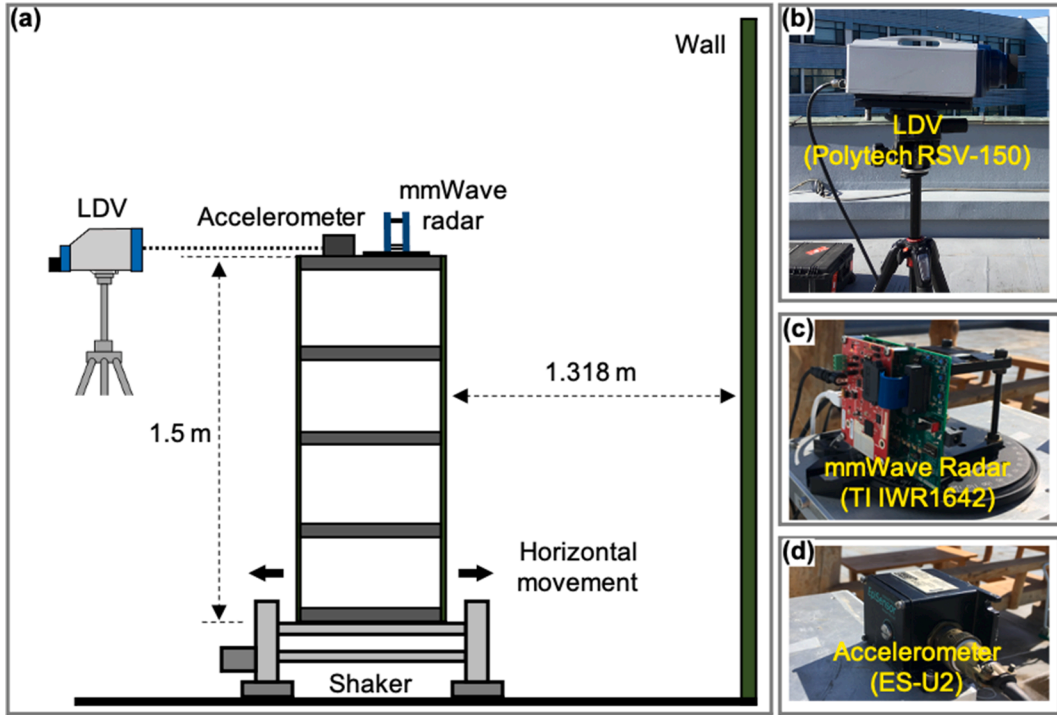
Fig. 8. Experimental setup for short-range displacement estimation test: (a) overview, (b) an LDV used for reference displacement measurement, (c) mmWave radar, and (d) accelerometer installed at the top of the building model.

3.3. FIR-filter-based displacement estimation by fusing radar-based displacement and acceleration

An FIR-filter-based technique has been developed for dynamic displacement estimation using acceleration measurements [7], and has been extended to fuse acceleration and inaccurate displacement measurements for displacement estimation with improved accuracy [13,15]. The FIR filter was adopted in this study to fuse the estimated radar-based displacement with acceleration measurements to further improve the displacement estimation accuracy.

Provided that the acceleration measurement (a) and radar-based displacement (u) are available within a given time window $[(k - M)\Delta t, (k + M)\Delta t]$,

$$a = [a_{k-M+1}, a_{k-M+2}, \cdots, a_{k+M-1}]^T \tag{17}$$

$$u = [u_{k-M}, u_{k-M+1}, \cdots, u_{k+M}]^T$$

An error function $\Pi\{u^*\}$ is defined for the final fusion-based displacement (u^*), as follows:

$$\Pi(u^*) = \frac{1}{2}\|L_a L_c u^* - L_a(\Delta t)^2 a\|_2^2 + \frac{\lambda^2}{2}\|u^* - u\|_2^2 \tag{18}$$

$$u^* = [u_{k-M}^*, u_{k-M+1}^*, \cdots, u_{k+M}^*]^T \tag{19}$$

where L_a and L_c denote the weighting matrix and second-order differential operator matrix, respectively. $\| \bullet \|_2$ denotes the two-norm of a vector, and λ is the regularization factor. The first item of Equation (18) denotes the error between a and the acceleration calculated from u^*, and the second item denotes the error between u^* and u. By minimizing $\Pi\{u^*\}$ with respect to u^*, u^* can be estimated as.

$$u^* = (\Delta t)^2 (L^T L + \lambda^2 I)^{-1} L^T L_a a + \lambda^2 (L^T L + \lambda^2 I)^{-1} u \tag{20}$$

$$L = L_a L_c$$

Because the highest estimation accuracy is achieved at the center of the time window $[(k - N)\Delta t, (k + N)\Delta t]$, only the displacement estimated at the center was retained,

$$u_k^* = C_H a + C_L u \tag{21}$$

Table 1
Radar specification and chirp configuration.

	Parameters (Units)	Specifications
mmWave Radar (TI IWR1642)	Start frequency (GHz)	77
	Bandwidth (GHz)	Up to 4
	Transmit power (dBm)	12.5
	RX Noise Figure (dB)	15
	Phase Noise at 1 MHz (dBc/Hz)	−93
	Operating Temp Range (°C)	–40 to 105
Chirp Signal	Frequency slope (MHz/µs)	64.985
	Number of ADC samples	256
	ADC sampling frequency (ks/s)	6000
	Chirp duration (Ramp end – Ramp start) (µs)	60

Fig. 9. Conversion factor estimation result.

where C_H and C_L denote the $(M+1)^{th}$ row of $\left\{ (\Delta t)^2 \left(L^T L + \lambda^2 I \right)^{-1} L^T L_a \right\}$ and $\left\{ \lambda^2 \left(L^T L + \lambda^2 I \right)^{-1} \right\}$, respectively. Note that C_H acts as double integration and high-pass filter, while C_L acts as low-pass filtering. Therefore, u_k^* is estimated as the combination of the high-frequency displacement from u and the low-frequency displacement from a. To estimate the displacement at the kth time step, radar-based displacement and acceleration measurements up to the $(k+M)^{th}$ time step are required, thus causing a time delay of $M\Delta t$. Further details can be found in the study of Lee *et al.* [7].

4. Four-story building model test

The proposed displacement estimation technique was first validated using a four-story building model. Two different experimental setups were considered for displacement estimation using long- and short-distance targets.

4.1. Short-range (1.318 m) test

First, the experiments were conducted using a short-range target. As shown in Fig. 8(a), an EpiSensor ES-U2 force balance accelerometer (Fig. 8(d)) and a TI IWR1642 mmWave radar (Fig. 8(c)) were placed on top of a four-story building model, and an APS 400 ELECTRO-SEIS shaker moved the model in the horizontal direction. A concrete wall located at a distance of approximately 1.318 m was selected as the fixed target for the radar. A Polytech RSV-150 LDV (Fig. 8(b)) measured the ground truth displacement of the model with a resolution of 0.3 nm [27]. All measurements from the radar, accelerometer, and LDV were obtained at a sampling rate of 100 Hz. The chirp configuration of the radar is listed in Table 1. With the given chirp configuration, the radar can detect targets up to a distance of 12 m with a resolution of 4.89 cm. Four different excitation signals were input into the shaker in this test: (1) 0.1 Hz, (2) 0.3 Hz, (3) 1 Hz sinusoidal inputs, and (4) a recorded real bridge vibration.

The best target was selected at the distance of 1.3137 m, and the conversion factor was estimated as $\beta_1 = 0.985$ using radar and acceleration measurements with 1 Hz sinusoidal inputs (Fig. 9). Note that the distance of the best target estimated from radar measurement is smaller than the perpendicular distance between the radar and the wall (1.318 m). Considering that the radar has only 4.89 cm distance resolution, these two distances are considered equal, and thereafter the existing algorithm [20] estimates the conversion factor as $\beta_2 = 1$ using Equation (9).

Radar-based displacements are first estimated using β_1 but with different phase-unwrapping algorithms (*i.e.,* the proposed and existing phase-unwrapping algorithms [26]) to examine the effectiveness of the proposed phase-unwrapping algorithm. As shown in Fig. 10, in all four cases, the proposed phase-unwrapping algorithm properly estimated displacements with RMSEs of the estimated displacements smaller than 0.32 mm. The existing phase-unwrapping algorithm assumes that the phase change between consecutive
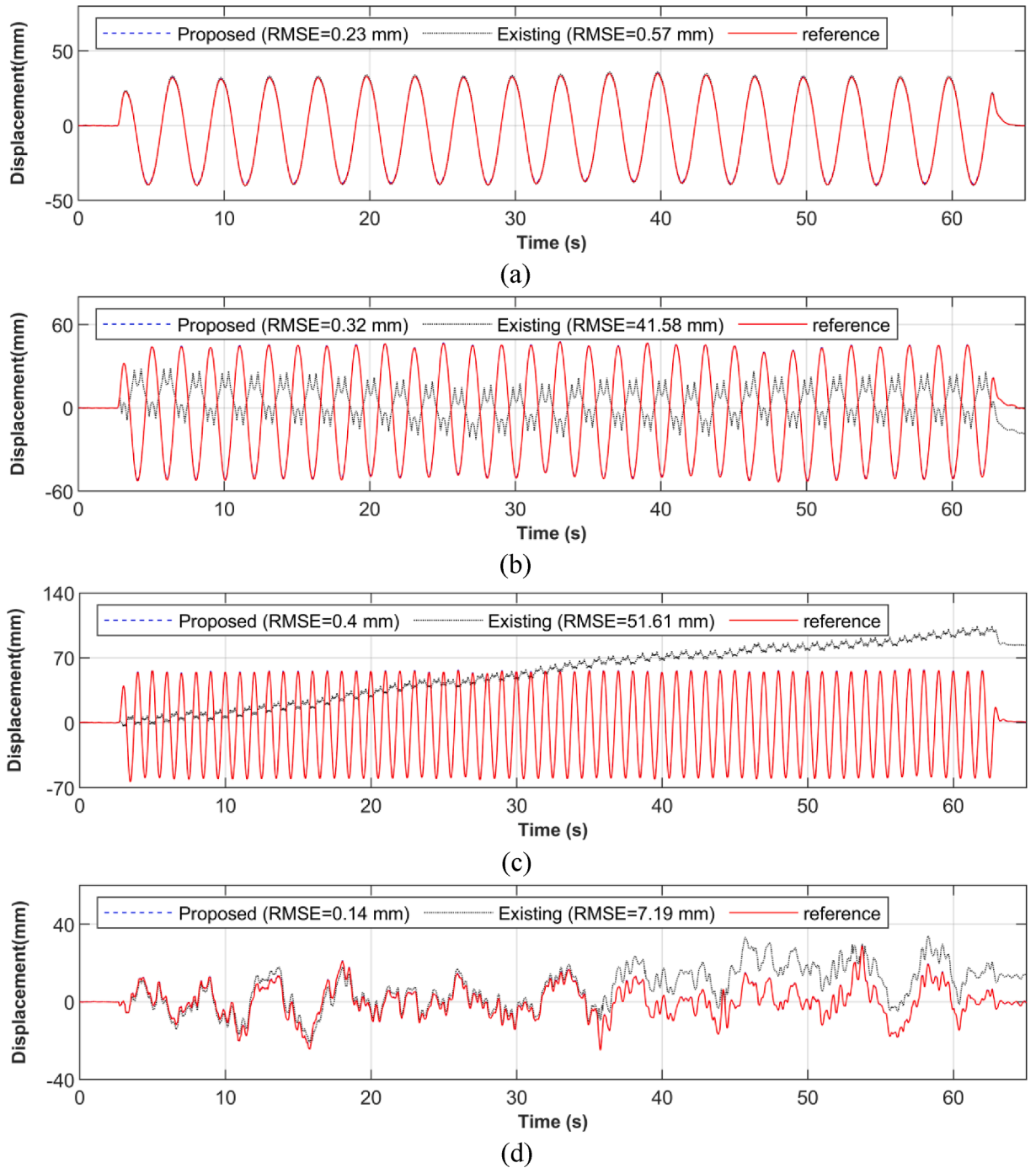
Fig. 10. Comparison of radar-based displacements estimated with the proposed and existing phase-unwrapping algorithms [26] when the four-story building model is subjected to (a) 0.3 Hz, (b) 0.5 Hz, (c) 1 Hz sinusoidal inputs, and (d) recorded real bridge vibration excitation signals.

time steps is smaller than π [26]. With a slowly changing displacement (*i.e.,* 0.3 Hz sinusoidal excitation), the displacement estimated using the existing phase-unwrapping algorithm is essentially the same as the reference displacement (Fig. 10(a)). However, when there are sudden phase changes (*i.e.,* 0.5 Hz, 1 Hz, and recorded real bridge excitations), the existing unwrapping algorithm fails to properly estimate displacement owing to the violation of the assumption. (Fig. 10(b), (c), and (d)).

Next, radar-based displacements were estimated using the proposed phase-unwrapping algorithm but with different conversion factors (*i.e.,* β_1 and β_2) to examine the effectiveness of the proposed conversion factor estimation algorithm. The use of β_1 reduced the RMSEs of the estimated displacements by approximately 38 %, as shown in Fig. 11(a). Finally, radar-based displacements estimated
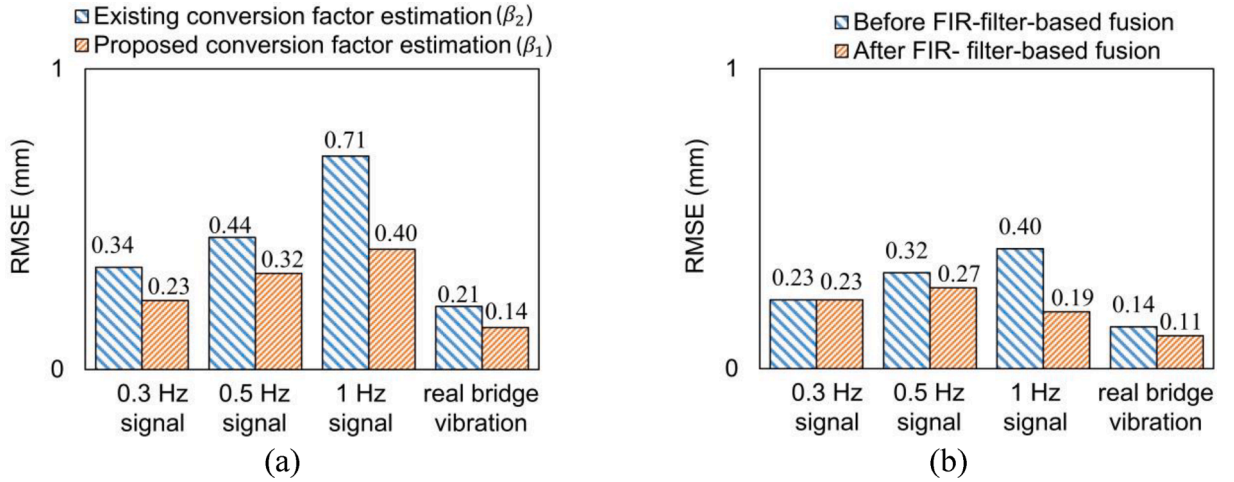
Fig. 11. (a) Accuracy improvement in radar-based displacement estimation using the proposed conversion factor estimation algorithm and (b) comparison of the displacement estimation performance before and after FIR-filter-based fusion in short-range test.
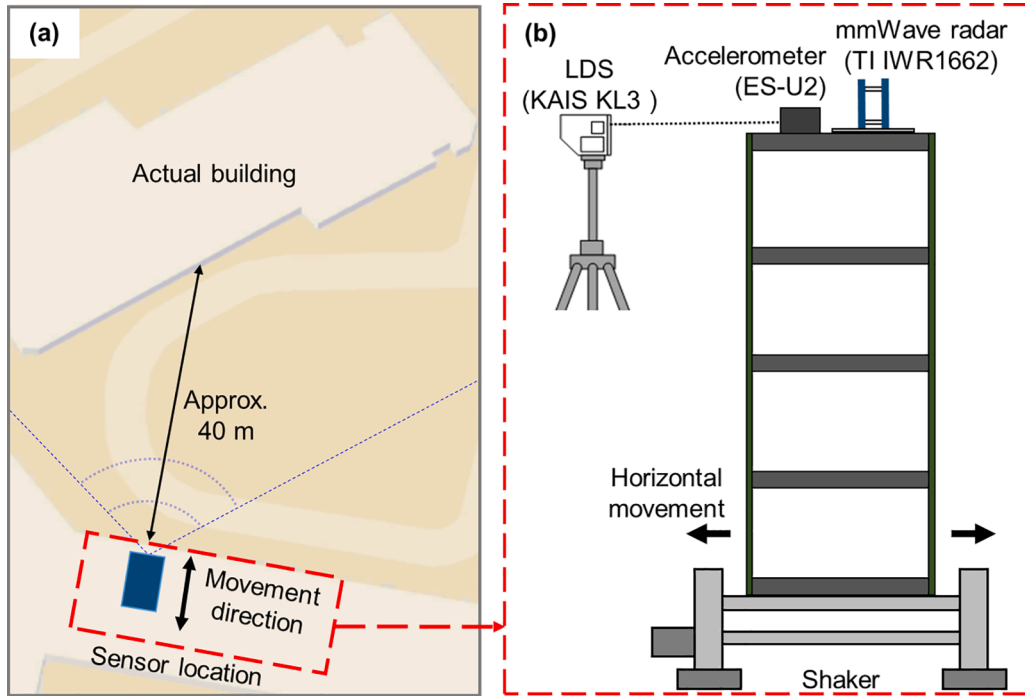

Fig. 12. Experimental setup for long-range test: (a) test location and (b) overview of sensor setup.

using β_1 and the proposed phase-unwrapping algorithm were fused with acceleration measurements using an FIR filter to obtain fusion-based displacements. The order of the FIR filter is set to 101 in this study, considering the noise characteristics of the radar and accelerometer, and thereafter a 0.5 s time delay is introduced. An RMSE reduction of approximately 27 % was achieved after the FIR-filter-based fusion (Fig. 11(b)).

4.2. Long-range (54 m) test

In practice, it is often difficult to find a fixed target near the radar for large-scale structures. For example, to estimate the displacement at the mid-span point of large-scale river-crossing bridges, the nearest target would be the foundation of the pylon, but it is at least a few tens of meters away from the radar installation location (*i.e.,* the mid-span point). The ability of high-accuracy displacement estimation with a long-distance target is important for the future practical application of the proposed technique.
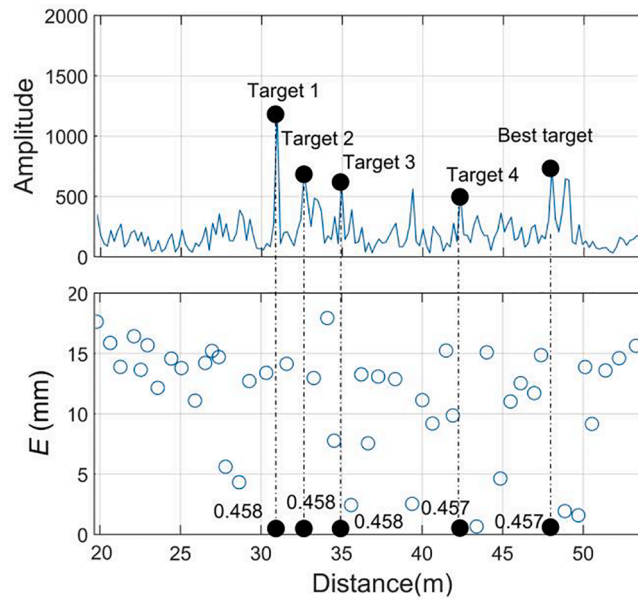
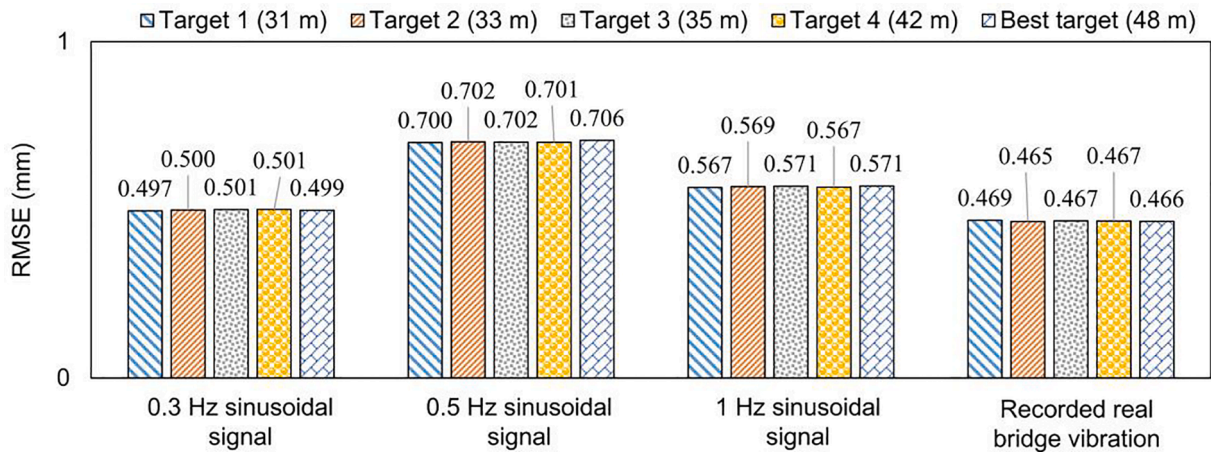Fig. 13. Best target selection result.

Fig. 14. Comparison of radar-based displacements estimated by the proposed technique using targets at different distances in long-range test.

Therefore, experiments were then conducted on the same building model considering long-distance targets (Fig. 12). An actual building located at a distance of approximately 30–60 m was selected as a fixed target for the radar system (Fig. 12(a)). The ground truth displacement was measured using a KAIS KL3-W400 laser displacement sensor (LDS) with a resolution of 10 μm [28]. The frequency slope of the chirp signal was changed from 64.985 MHz/μs to 15.015 MHz/μs, and the radar could detect targets up to a distance of 54 m with a resolution of 21 cm. Unless otherwise stated, all other test parameters remained the same as those used in the previous short-range tests.

The best target is automatically selected at a distance of 48 m, but the other four targets (labeled targets 1–4) at distances of 31–42 m have approximately identical E values, as shown in Fig. 13. Using the proposed conversion factor estimation and phase-unwrapping algorithms, the displacements estimated from these five targets are compared in Fig. 14. Although the distances from the radar to these targets were different, almost identical displacement estimation performances were achieved.

The effectiveness of the proposed phase-unwrapping algorithm was examined by comparing the radar-based displacements estimated using the best target and the proposed conversion factor estimation algorithm. The proposed phase-unwrapping algorithm properly estimates displacements once again, for all four excitations, while the existing phase-unwrapping algorithm properly estimates displacements only at 0.3 Hz sinusoidal excitation (Fig. 15(a)). The radar-based displacements estimated using the best target, the proposed conversion factor estimation, and phase-unwrapping algorithms were further fused with acceleration measurements using the FIR filter, and an RMSE reduction of approximately 11 % was achieved (Fig. 15(b)).
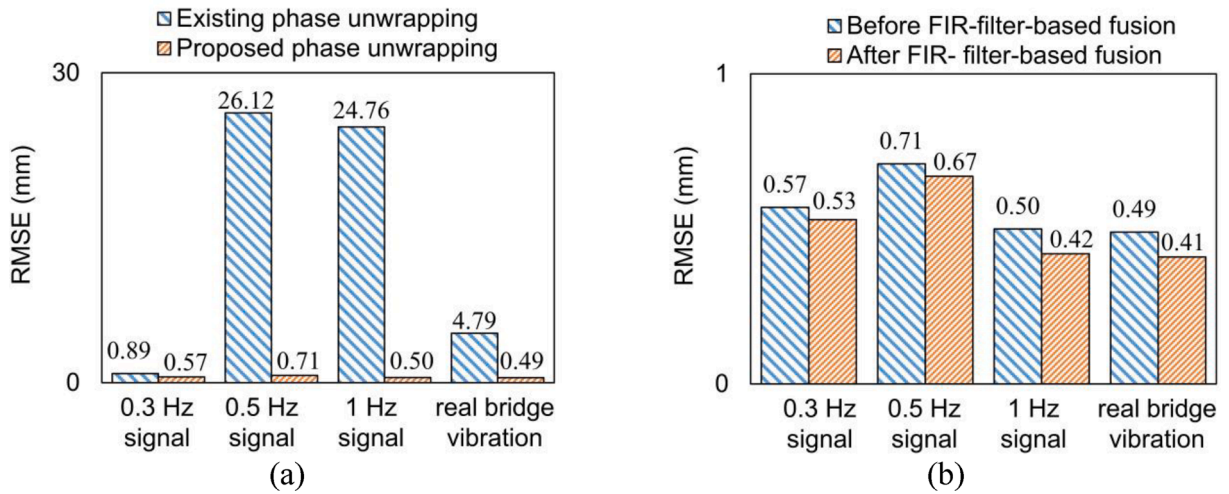
Fig. 15. (a) Accuracy improvement in radar-based displacement estimation using the proposed phase unwrapping algorithm and (b) comparison of the displacement estimation performance before and after FIR-filter-based fusion in long-range test.
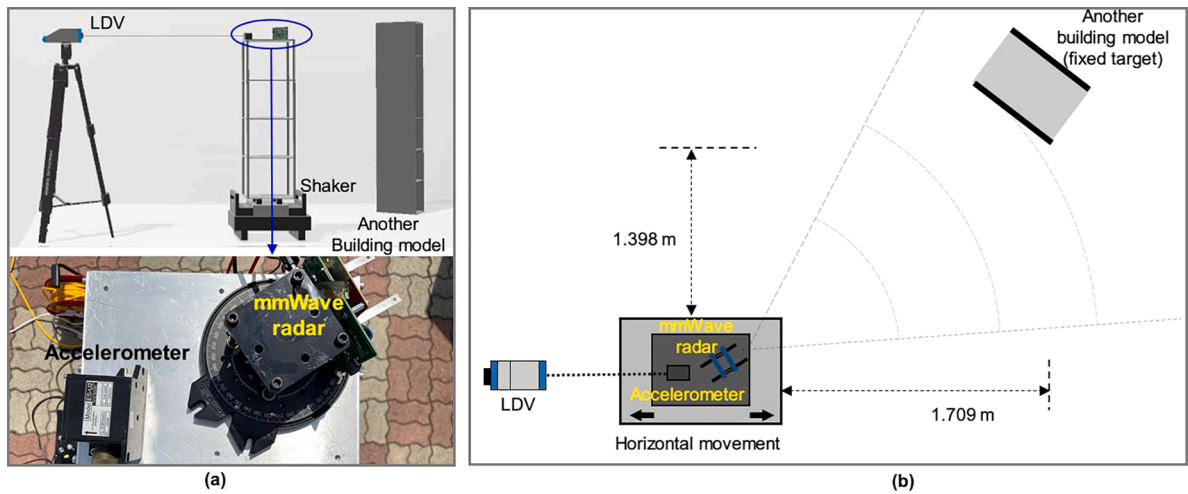

Fig. 16. Overview of experimental setup considering the deviation between LOS and actual movement directions: (a) front view and (b) top view.
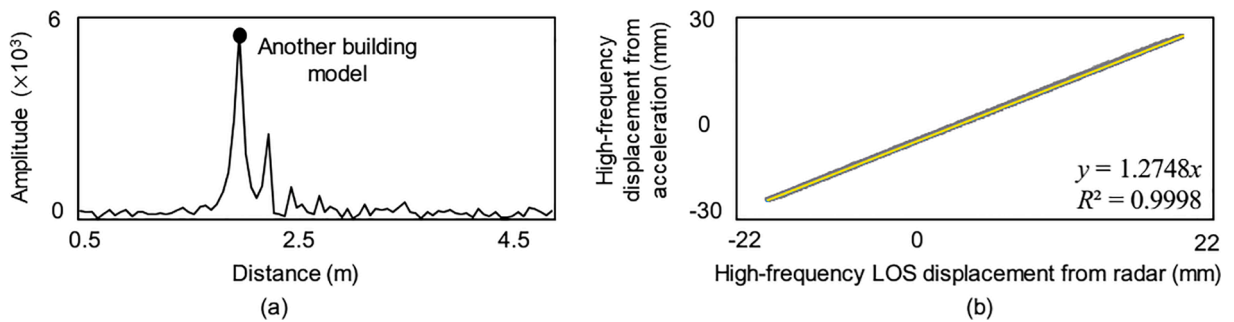

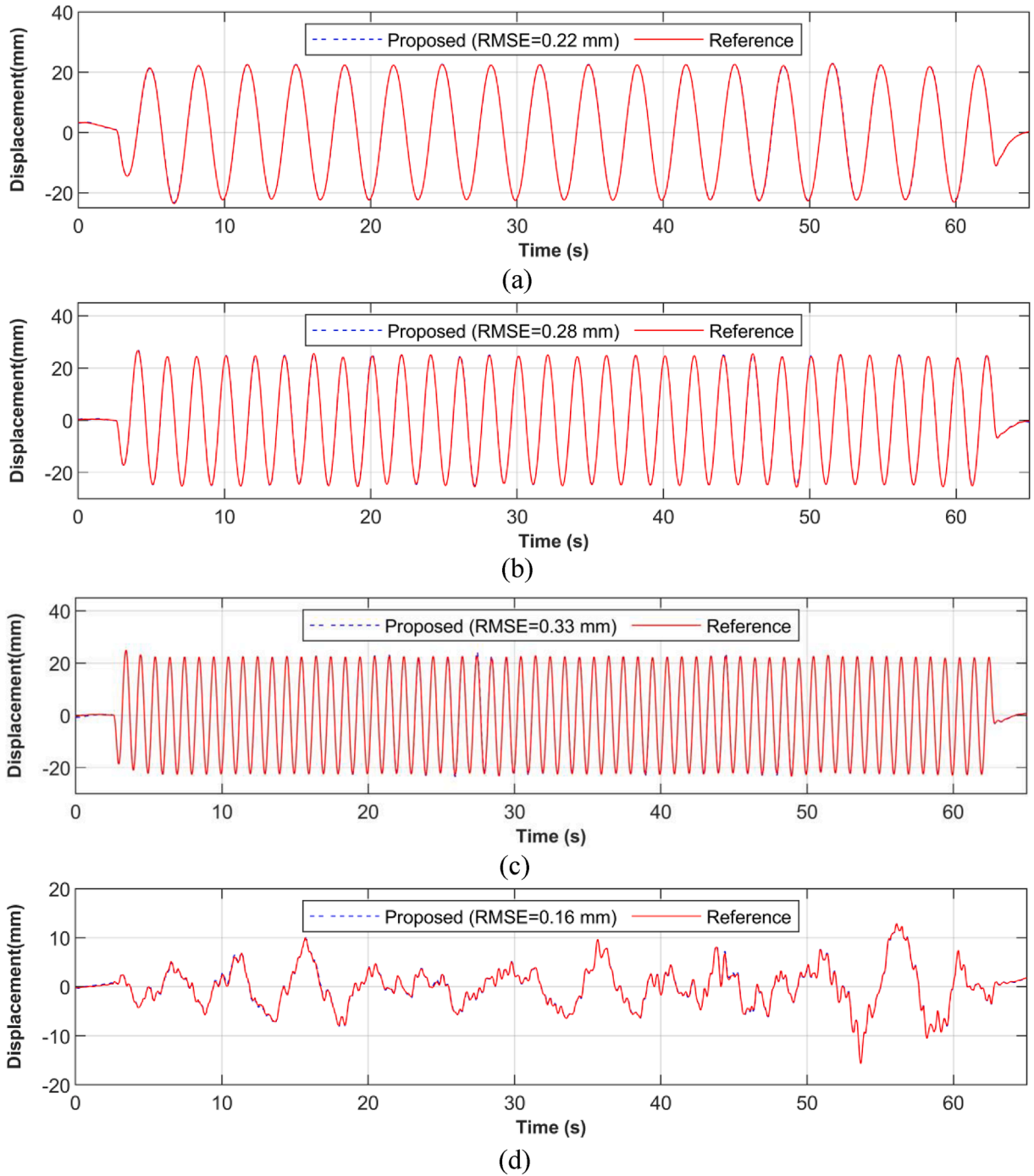**Fig. 17.** (a) Targets detected by the radar and (b) conversion factor estimation result.

Fig. 18. Final displacements estimated by the proposed technique considering the deviation between LOS and actual movement directions.

4.3. Additional test considering the deviation between LOS and actual movement directions

In the previous two tests, the LOS direction of the best target basically coincides with the actual structural vibration direction. However, when measuring displacement on river-crossing bridges, the unstable water surface cannot be used as the best target. Then, the LOS direction of the best target will deviate from the actual bridge vibration direction as shown in Fig. 4(a). An additional test was performed using the experimental setup shown in Fig. 16. Except that another building model instead of the wall was used as a target, the experimental setup is identical to that used in the short distance test.

Fig. 17(a) shows the target detected by the radar. The additional building model was detected at a distance of 2.0543 m, and
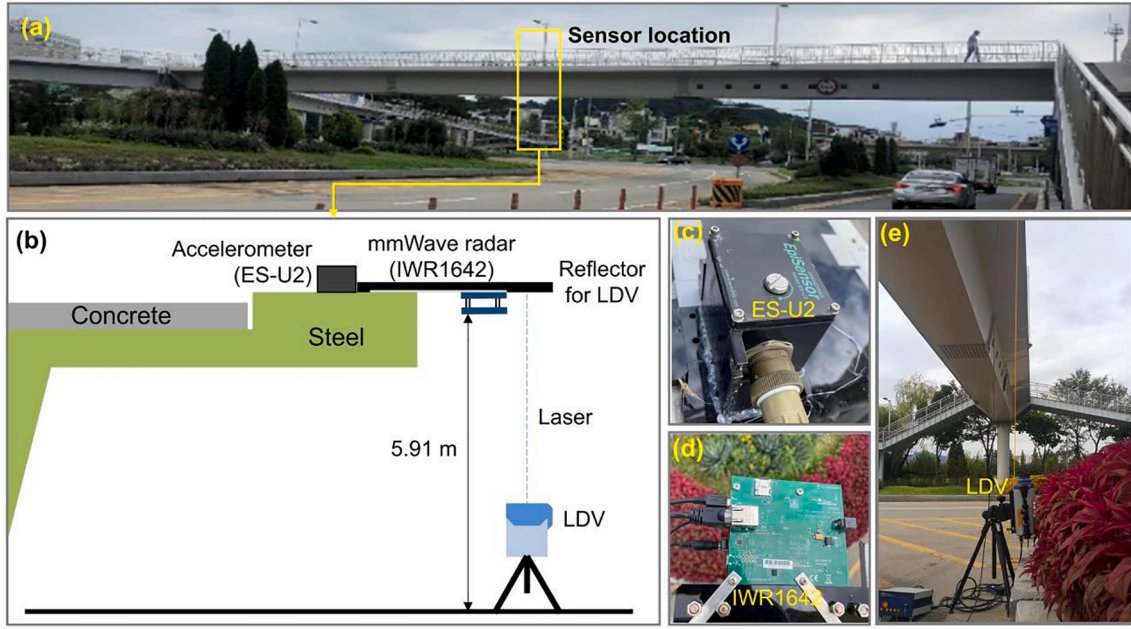
Fig. 19. Pedestrian bridge test: (a) bridge overview, (b) overview of sensor setup, (c) an accelerometer, (d) a mmWave radar, and (e) an LDV for reference displacement measurement.
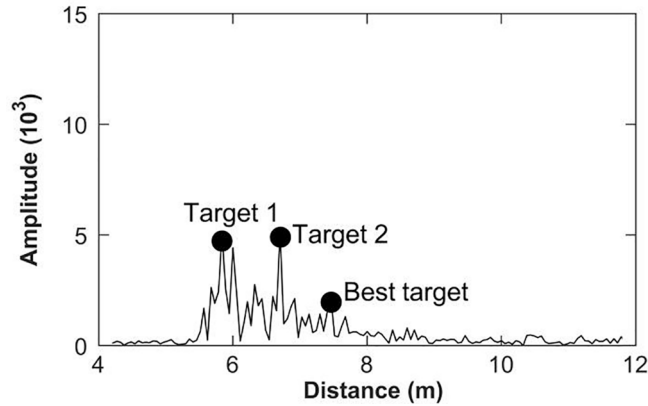

Fig. 20. Target detected by radar and the best target automatically selected by the proposed algorithm in pedestrian bridge test.

selected as the best target. The conversion factor was estimated as 1.2748, and a good linear relationship was found between the high-frequency displacement from acceleration and high-frequency LOS displacement from radar as shown in Fig. 17(b).

Fig. 18 shows the final displacements estimated by the proposed technique. Though the LOS direction deviates from the structural actual movement direction, the proposed technique still estimates displacement accurately with RMSEs less than 0.4 mm. Note that the effectiveness of the proposed conversion factor estimation, best target selection, and accelerometer-aided phase unwrapping algorithms have been verified in the previous two tests, and then similar results were not repeatedly reported here.

5. Pedestrian bridge test

A pedestrian bridge test was conducted to further validate the proposed technique. The experimental setup is shown in Fig. 19. The same mmWave radar (Fig. 19(d)) and accelerometer (Fig. 19(c)) were installed at the one-half span of the bridge, as in the previous tests. A Polytech RSV-150 LDV was installed under the bridge to measure the ground truth displacement of the bridge (Fig. 19(e)). Note that LDV has following limitations, and then is not a good option for continues displacement monitoring of practical structures: (1) securing a permeant installation location for long-term monitoring can be challenging; (2) cabling for permanent power supply and data retrieval can be issues; (3) A reflector with retroreflective film should be installed at displacement estimation location, and the laser beam should be perpendicular to the reflector surface to ensure a stable reflection; (4) the LDV is rather expensive; (5) long
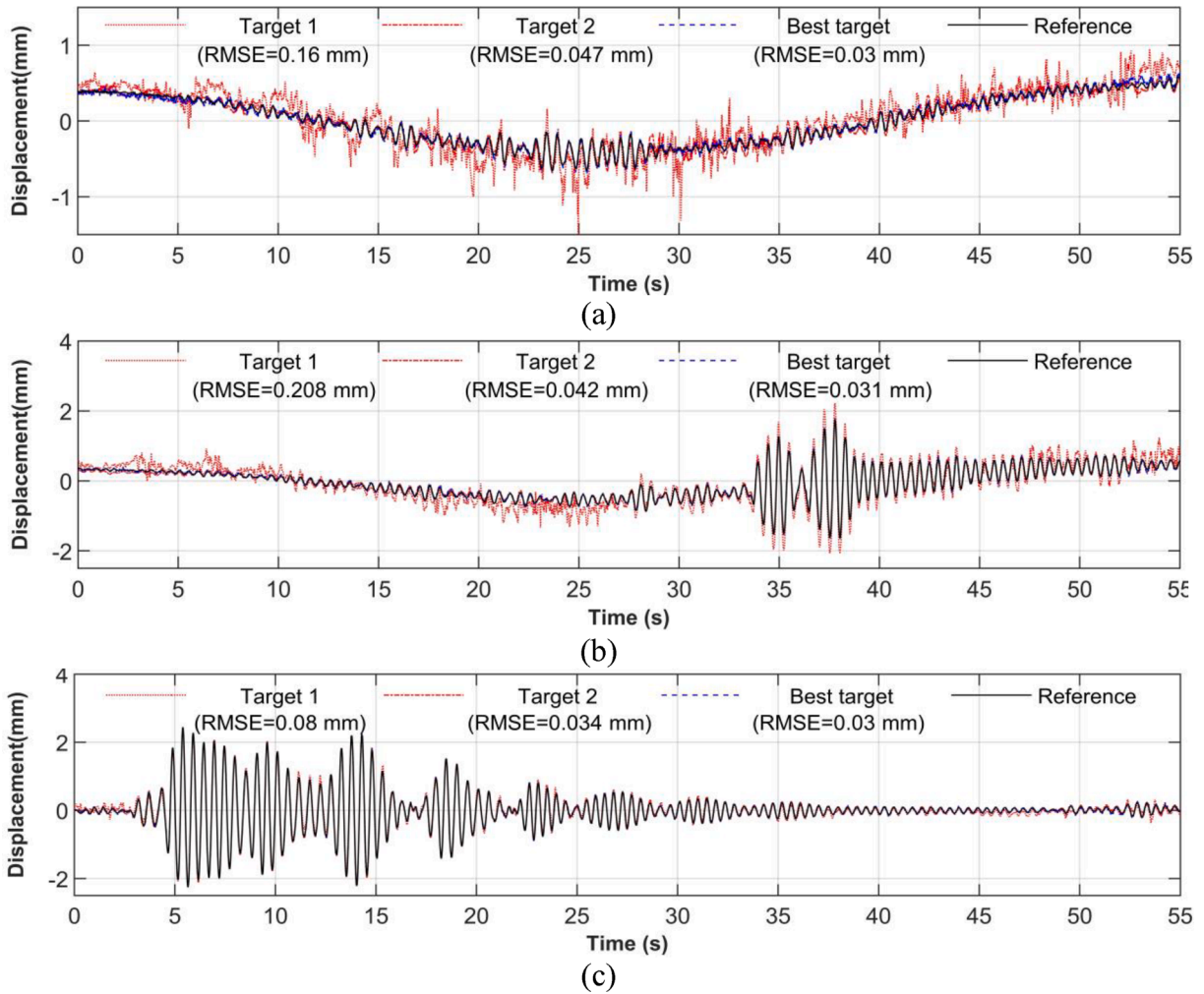
Fig. 21. Comparison of radar-based displacements estimated using three different targets in pedestrian bridge test: (a) 14 people slowly passing, (b) 14 people slowly passing +5 people jumping, and (c) 6 people jumping.
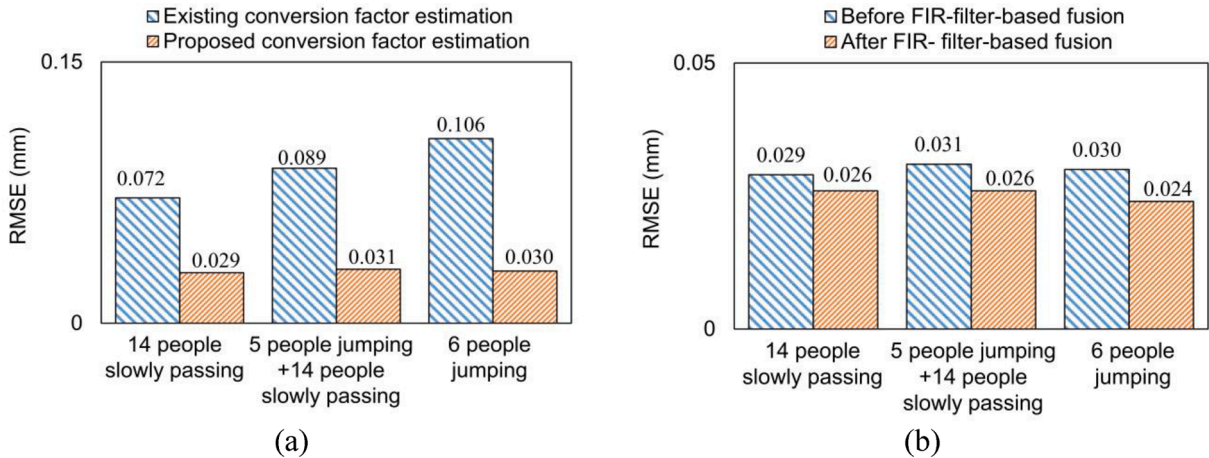

Fig. 22. (a) Accuracy improvement in radar-based displacement estimation using the proposed conversion factor estimation algorithm and (b) comparison of the displacement estimation performance before and after FIR-filter-based fusion in pedestrian bridge test.
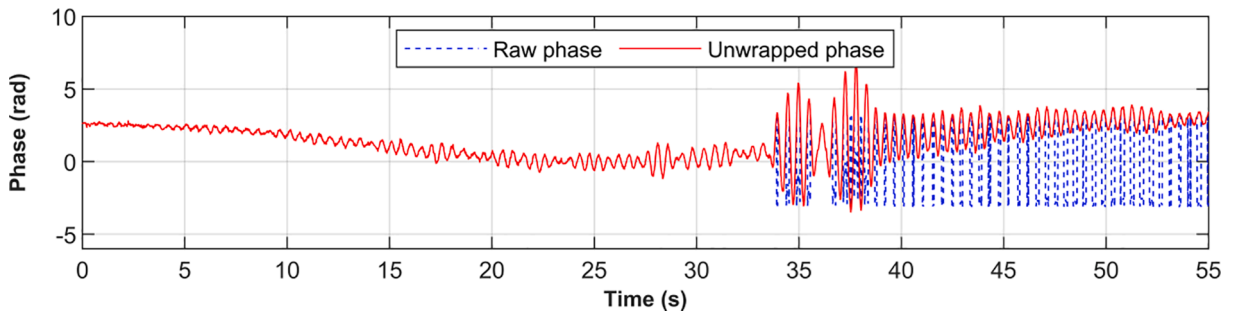
Fig. 23. Comparison of raw phase and unwrapped phase recovered by the proposed phase-unwrapping algorithm when 14 people slowly passing the bridge and 5 people jumping at one-half span point.

distance measurement requires the use of a high-intensity laser beam that would endanger human health [29].

The chirp configuration of the radar system was the same as that in the previous short-range building model test, and the radar could detect targets with a maximum distance of 12 m and a distance resolution of 4.89 cm. In this test, the bridge vibration was excited by (1) 14 people slowly passing the bridge, (2) 14 people slowly passing the bridge and 5 people jumping at the one-half span point, and (3) 6 people jumping at the one-half span point.

The target detection result of the radar is shown in Fig. 20, and the best target is automatically selected at a distance of 7.4605 m. Note that it is intuitive to choose the target with the largest amplitude; however, the best target does not have the largest amplitude in this test. Two other targets with larger amplitudes (labeled targets 1 and 2) were used to examine the effectiveness of the proposed best target selection algorithm. The displacements were estimated from these three targets using the proposed phase-unwrapping and conversion factor estimation algorithms. As shown in Fig. 21, using the best target estimates the displacements with the smallest RMSEs for all three excitations.

Radar-based displacements estimated using the proposed phase-unwrapping algorithm, but with two different conversion factor estimation algorithms, are compared in Fig. 22(a). For all three excitations, the proposed algorithm produces smaller RMSEs. The radar-based displacements estimated using the best target, the proposed conversion factor estimation, and phase-unwrapping algorithms were further fused with acceleration measurements using the FIR filter, and an RMSE reduction of approximately 16 % was achieved (Fig. 22(b)).

Fig. 23 compares the raw and unwrapped phases after using the proposed phase-unwrapping algorithm with 14 people slowly passing the bridge and 5 people jumping at the one-half span point. Phase wrapping occurs when the phase is larger than π or smaller than $-\pi$. Because the bridge displacements are small, up to 3 mm, as shown in Fig. 21, the assumption of the existing phase-unwrapping algorithm [26] is valid in the bridge test, and both the existing and proposed phase-unwrapping algorithms produce the same phase-unwrapping results.

6. Conclusions

This study proposed a displacement estimation technique through the fusion of a collocated FMCW mmWave radar and an accelerometer on a structure. An automated initial calibration is first performed to select the best target among all targets detected by radar from the surroundings of the structure and estimate a conversion factor for the best target. Thereafter, the displacement was initially estimated from radar measurements in real time using the selected best target and its estimated conversion factor. An accelerometer-aided phase-unwrapped algorithm was developed and applied in the radar-based displacement estimation process to address the phase-wrapping issue. The real-time estimated displacement from radar measurement is further fused with acceleration measurement to estimate a fusion-based displacement with an improved accuracy at the cost of short time delay (0.5 s in this study). The displacement estimation performance of the proposed technique was experimentally validated through laboratory tests on a four-story building model and a field test on a pedestrian bridge. The overall RMSEs of both the radar- and fusion-based displacements for all cases investigated in this study were less than 1 mm. Although the proposed technique shows a potential for practical applications in long-term continuous structural displacement monitoring, there are still limitations that need to be addressed. Firstly, the presented tests estimated displacement using a target distance of up to 48 m, which may not be sufficient for long-span bridges. In addition, LOS blockage issue may occur in long term continuous displacement monitoring, especially for bridges with intermittent traffic underneath. Future works are warranted to further advance displacement measurement range and address the LOS blockage issue.

Declaration of Competing Interest

The authors declare that they have no known competing financial interests or personal relationships that could have appeared to influence the work reported in this paper.

Acknowledgements

References

[1] AASHTO, AASHTO LRFD Bridge Design Specifications, in: the American Association of State Highway and Transportation Officials, Washington, D.C., 2017.

[2] MLTM, Korea highway bridge design code (in Korean), in: Ministry of Land, Infrastructure and Transport, Seoul, 2010.

[3] MOHURD, GB 50017–2017 Code for Design of Steel Structures (in Chinese), in: China Machine Press, Beijing, 2020.

[4] M.A. Vicente, D.C. González, G. Fu, Static and dynamic testing of high-speed rail bridges in Spain, J. Bridge Eng. 20 (2015) 06014006, https://doi.org/10.1061/(ASCE)BE.1943-5592.0000654.

[5] S. Bhowmick, S. Nagarajaiah, Spatiotemporal compressive sensing of full-field Lagrangian continuous displacement response from optical flow of edge: Identification of full-field dynamic modes, Mech. Syst. Sig. Process. 164 (2022), 108232.

[6] M. Civera, L.Z. Fragonara, C. Surace, A computer vision-based approach for non-contact modal analysis and finite element model updating, in: P. Rizzo, A. Milazzo (Eds.), European Workshop on Structural Health Monitoring, Springer International Publishing, Cham, 2021, pp. 481–493.

[7] H.S. Lee, Y.H. Hong, H.W. Park, Design of an FIR filter for the displacement reconstruction using measured acceleration in low-frequency dominant structures, Int. J. Numer. Meth. Eng. 82 (2010) 403–434, https://doi.org/10.1002/nme.2769.

[8] F. Moreu, J. Li, H. Jo, R.E. Kim, S. Scola, B.F. Spencer, J.M. LaFave, Reference-free displacements for condition assessment of timber railroad bridges, J. Bridge Eng. 21 (2016) 04015052.

[9] A.I. Ozdagli, B. Liu, F. Moreu, Low-cost, efficient wireless intelligent sensors (LEWIS) measuring real-time reference-free dynamic displacements, Mech. Syst. Sig. Process. 107 (2018) 343–356.

[10] M. Gindy, R. Vaccaro, H. Nassif, J. Velde, A state-space approach for deriving bridge displacement from acceleration, Comp.-Aided Civil Infrastr. Eng. 23 (2008) 281–290, https://doi.org/10.1111/j.1467-8667.2007.00536.x.

[11] K. Kim, J. Choi, J. Chung, G. Koo, I.-H. Bae, H. Sohn, Structural displacement estimation through multi-rate fusion of accelerometer and RTK-GPS displacement and velocity measurements, Measurement 130 (2018) 223–235, https://doi.org/10.1016/j.measurement.2018.07.090.

[12] Z. Ma, J. Chung, P. Liu, H. Sohn, Bridge displacement estimation by fusing accelerometer and strain gauge measurements, Struct. Control Health Monitor.. 28 (2021), e2733, https://doi.org/10.1002/stc.2733.

[13] J.-W. Park, S.-H. Sim, H.-J. Jung, Displacement estimation using multimetric data fusion, IEEE-ASME Trans. Mechatr. 18 (2013) 1675–1682, https://doi.org/10.1109/TMECH.2013.2275187.

[14] Y. Xu, J.M. Brownjohn, F. Huseynov, Accurate deformation monitoring on bridge structures using a cost-effective sensing system combined with a camera and accelerometers: Case study, J. Bridge Eng. 24 (2019) 05018014, https://doi.org/10.1061/(ASCE)BE.1943-5592.0001330.

[15] Y.H. Hong, S.G. Lee, H.S. Lee, Design of the FEM-FIR filter for displacement reconstruction using accelerations and displacements measured at different sampling rates, Mech. Syst. Sig. Process. 38 (2013) 460–481, https://doi.org/10.1016/j.ymssp.2013.02.007.

[16] J. Kim, K. Kim, H. Sohn, Autonomous dynamic displacement estimation from data fusion of acceleration and intermittent displacement measurements, Mech. Syst. Sig. Process. 42 (2014) 194–205.

[17] A. Smyth, M. Wu, Multi-rate Kalman filtering for the data fusion of displacement and acceleration response measurements in dynamic system monitoring, Mech. Syst. Sig. Process. 21 (2007) 706–723, https://doi.org/10.1016/j.ymssp.2006.03.005.

[18] Z. Ma, J. Choi, P. Liu, H. Sohn, Structural displacement estimation by fusing vision camera and accelerometer using hybrid computer vision algorithm and adaptive multi-rate Kalman filter, Autom. Constr. 140 (2022), 104338, https://doi.org/10.1016/j.autcon.2022.104338.

[19] Z. Ma, J. Choi, H. Sohn, Real-time structural displacement estimation by fusing asynchronous acceleration and computer vision measurements, Comp.-Aided Civil Infr. Eng. 37 (2022) 688–703, https://doi.org/10.1111/mice.12767.

[20] G. Zhang, Y. Wu, W. Zhao, J. Zhang, Radar-based multipoint displacement measurements of a 1200-m-long suspension bridge, ISPRS J. Photogramm. Remote Sens. 167 (2020) 71–84, https://doi.org/10.1016/j.isprsjprs.2020.06.017.

[21] S. Guan, J.A. Rice, C. Li, Y. Li, G. Wang, Structural displacement measurements using DC coupled radar with active transponder, Struct. Control Health Monit. 24 (2017), e1909.

[22] S. Guan, J.A. Bridge, C. Li, N.J. DeMello, Smart radar sensor network for bridge displacement monitoring, J. Bridge Eng. 23 (2018) 04018102.

[23] D.V.Q. Rodrigues, D. Zuo, C. Li, Wind-induced displacement analysis for a traffic light structure based on a low-cost doppler radar array, IEEE Trans. Instrum. Meas. 70 (2021) 1–9, https://doi.org/10.1109/TIM.2021.3098380.

[24] J. Guo, Y. He, C. Jiang, M. Jin, S. Li, J. Zhang, R. Xi, Y. Liu, Measuring micrometer-level vibrations with mmWave radar, IEEE Trans. Mob. Comput. 1–1 (2021).

[25] H. Liu, Robot Systems for Rail Transit Applications, Elsevier, 2020.

[26] G. Wang, J.-M. Munoz-Ferreras, C. Gu, C. Li, R. Gomez-Garcia, Application of linear-frequency-modulated continuous-wave (LFMCW) radars for tracking of vital signs, IEEE Trans. Microw. Theory Tech. 62 (2014) 1387–1399, https://doi.org/10.1109/TMTT.2014.2320464.

[27] Polytech GmbH, RSV-150 Scanning Vibrometer Datasheet, (2019). https://www.atecorp.com/products/polytec/rsv-150 (accessed March 24, 2022).

[28] KAIS Co., Ltd, KL3 series Laser Displacement Sensor Datasheet, (2019). https://ekais.kr/ekaisbiz/wp-content/uploads/2019/05/KL3-Series.pdf (accessed October 9, 2021).

[29] H.H. Nassif, M. Gindy, J. Davis, Comparison of laser Doppler vibrometer with contact sensors for monitoring bridge deflection and vibration, NDT and E Int. 38 (2005) 213–218, https://doi.org/10.1016/j.ndteint.2004.06.012.